Numerical and experimental test on a large scale model of a pivoting wave energy conversion system

Domenico P. Coiro, Giancarlo Troise, Nadia Bizzarrini, Luca Castellini and Guido Lazzerini

Abstract— **This paper presents the main results and on-going activities related to the development of an innovative system for converting mechanical energy from waves directly to electricity. It consists of a point pivoted body which oscillates in presence of waves. The PTO (power take-off) system is linked to the oscillating arms connecting a floating body to the pivoting hinge. A ballscrew based electro-mechanical actuator/generator converts floating movements (the mechanical power captured by the buoyant body) induced by waves into electrical power. Thanks to the WEC kinematic, buoy rotational motion is converted into linear movements at the absorber. The prime mover, represented by the pivoting buoy, and the PTO system have been integrated with the aim to optimize the overall system behaviour. Experimental results on both small scale and full-scale models are presented, together with the numerical model results used during project development.**

Keywords— **Pivoted wave actuated body, recirculating ball-screw PTO, wave energy.**

I. Introduction

THE work presented in this paper is related to the development of a wave energy device based on a pivoting buoy associated with an electromechanical power take-off (PTO) system based on the recirculating ball-screw technology integrated with an electric generator.

Wave energy is one of the most attractive sources of renewable energy, mainly for the high potentially available resource. Several concepts have been presented and many studies can be found in literature with respect to different solutions for harnessing wave energy. General aspects on wave energy converters may be found in [1].

The presented device may be classified as a wave actuated body oscillating under wave action around a fixed hinge. Several research activities have been presented in literature on similar topics. In particular, the subject of wave actuated bodies has been extensively studied in literature. Point absorbers in heave, for example, represent a common type of wave energy converter (WEC) and many analytical studies (see for example [1]) as well as numerical and experimental researches have been reported (see for example [2], [3]). The concept and modelling of hinged WECs has been explored for example in [4], [5] and [6].

In the present case study, the prime mover of the system is composed by a pivoting floating body (buoy) oscillating under wave action. The PTO has a piston rod connected at one end to the oscillating body. A schematic view of the system is reported in Fig. 1.

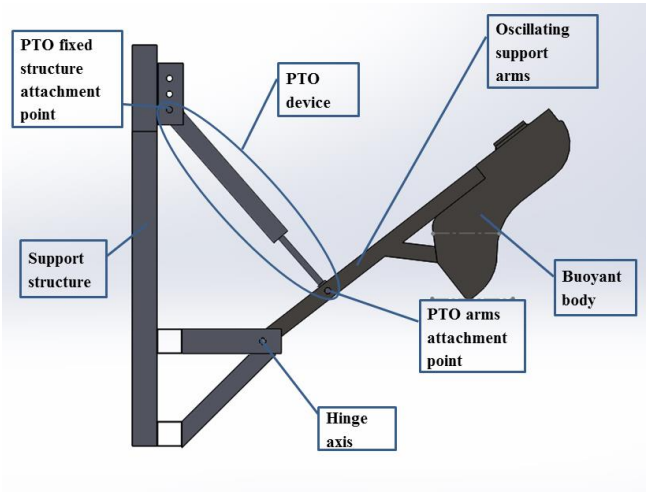

Fig. 1. Schematic view of the system structure.

A proper kinematic arrangement allows the transformation of the alternated rotational motion of the floating body in a linear motion, fed as input to the PTO, which in turn actuates an electric generator integrated into a suitably developed ball-screw mechanism. The floating body (buoy) is connected to a main oscillation hinge, placed under the water level by means of oscillating

This paper, with ID 1659, has been submitted in the EWTEC conference track "Wave device development and testing". This work was supported in part by a regional funding partially by the WES (Wave Energy Scotland) and partially by the Italian Development Ministry (MISE) funding under gran agreement F/050251/01-03/X32.

D. P. Coiro is full professor at the University of Naples "Federico II", via Claudio 21, Napoli, Italy (e-mail: coiro@unina.it).

G. Troise and Nadia Bizzarrini work at Seapower scrl, Via Giuseppe Fiorelli, 14, 80121, Napoli, Italy (e-mail: g.troise@seapowerscrl.com, n.bizzarrini@seapowerscrl.com).

G. Lazzerini is with Department of Industrial Engineering, University of Naples "Federico II", via Claudio 21, Napoli, Italy (e-mail: guido.lazzerini@gmail.com).

L. Castellini works at Umbra Group Spa.

 Copyright © European Tidal and Wave Energy Conference 2019

support arms. The PTO is linked to the support arms at one end and suspended at a fixed hinge at the other end. The whole PTO device, with the integrated generator, oscillates during the motion of the system.

It may be noted, however, that other possible PTO solutions may be coupled with the same pivoting buoy concept.

The prime mover, represented by the pivoting buoy, has been developed by Seapower in cooperation with the University of Naples, while the PTO system has been designed and manufactured by Umbra Group Spa: the two main components have been integrated with the aim to optimize the overall system behaviour.

A further development of the project involves the installation of a prototype in real sea environment. The demonstrator will be deployed on a breakwater installed in a harbour area. Among other problems observed during the development of the system, the issues related to breakwater wave reflection and to the behaviour in extreme wave conditions have to be taken into account and will be highlighted in the paper. Some of the project related advancements will be addressed in the following paragraphs.

II. NUMERICAL MODEL

A. System response simulation

The dynamic behaviour of the system may be described to a first order of approximation by the use of a simple equivalent 1DOF equation that represents the equilibrium of moments around the hinge axis:

$$I\ddot{\theta} = M_{exc} + M_{rad} + M_0 + M_{PTO} \quad (1)$$

where:

- I is the rotational inertia around the hinge axis (accounting for the hydrodynamic added mass also);
- M_{exc} is the external moment due to waves excitation forces (diffractive and Froude-Krylov forces);
- M_{rad} is a term accounting for the radiation force, which should be corrected for viscous contribution;
- M_0 is a term related to hydrostatic stiffness;
- M_{PTO} is the moment due to the point pivoted power take-off device (PTO);
- θ is the inclination angle of the support arm of the body.

For the estimation of the wave-body interaction, different approaches may be used with different degrees of accuracy. A mid-fidelity approach is based on the use of the classic potential flow theory, which may give an estimation of the excitation and radiation forces. Codes based on the potential flow theory may be used for the calculation of the frequency dependent hydrodynamic coefficients (excitation force, added mass and radiation damping) for each degree of freedom. Such coefficients may be used to estimate the wave actions both in regular and irregular sea states. Detailed information about the determination and use of hydrodynamic coefficients may be found in several references (see for example, [7] or [8]).

A different high-fidelity approach to model wave body interactions is based on CFD analyses. Although such method is able to provide a higher accuracy in the estimation of wave actions, it also has a higher computational cost, requiring both a large amount of resource and a longer simulation time.

In order to model the correct behaviour of the system, an assumption has to be made regarding the control law defining the PTO action. The choice of a proper control law has a significant impact on the performances of the device. In the present study for the control law, a linear relation between the force, F_p, acting on the PTO piston and the piston oscillation velocity, v_p , has been considered, according to the following expression:

$$F_p = K v_p \quad (2)$$

The force-speed gain, K, in the assumed control law, is one of the major parameters affecting the response of the system.

A validation of the model has been performed by comparison with the experimental results of a test campaign on a small-scale model (with a 1 m wide floating body). The comparison is reported with respect to the free oscillations of the system under wave action, considering no PTO reaction loads or other damping actions. A potentiometer was used to measure the distance variation between the two PTO attachment points (with no reacting load applied). For comparison purposes, the results of a CFD model are also reported. The model was developed through the commercial code StarCCM+™, considering unsteady biphasic RANS equations coupled with the rigid body dynamics of the buoy, and is not described in details in this paper for brevity.

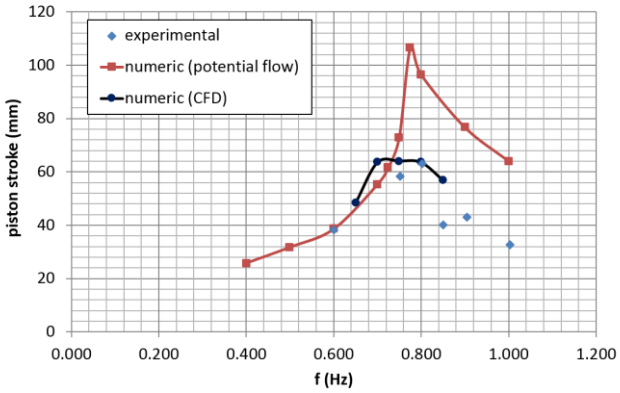

Fig. 2. Comparison of potential flow, CFD and experimental results in terms of piston oscillation amplitude as a function of wave frequency with no PTO load.

The commercial code Ansys AQWA™ was used for the determination of the hydrodynamic coefficients. The potential flow analyses were performed neglecting the effect of the tank walls. A preliminary CFD study, not

reported here for brevity, seems to confirm a negligible influence of the tank side walls at least for the tested condition. Further works are planned to investigate this topic.

As can be seen a large overestimation of the effective response is predicted by the potential flow simulations. Such difference is probably explainable considering that the potential flow theory completely neglects the viscous effects, which may be significant particularly for small scale models. For larger models a reduced discrepancy may be expected.

Nonetheless, despite the lack in accuracy of the potential flow simulations, this approach has been used in optimizations analyses in consideration of the reduced computational cost, which is of primary importance when a large number of analyses are required as in the design phase or in simulation-based optimization procedures.

More details on the small-scale model experimental campaign and on the performed numerical analyses may be found in [9].

With respect to the PTO control law, besides the assumption on the linear relation between piston force and speed, a more complex model of the PTO reaction force has been implemented in order to take into account the so-called "back-drive" force, characteristic of ball-screw devices. Specifically, the following relation has been assumed to model the total PTO action, $F_{p\,tot}$:

$$F_{p\,tot} = F_p + F_{backdrive} \tag{3}$$

$$F_{backdrive} = -K_{visc} v_p - F_{friction} \cdot sign(v_p) - K_{inertia} a_p \tag{4}$$

where K_{visc} represent a viscous contribution, $F_{friction}$ a coulombian friction contribution and $K_{inertia}$ an equivalent inertia term proportional to piston acceleration, a_p.

Values for the coefficients needed for the definition of the back-drive force have been found by experimental bench test performed by the PTO supplier.

The outputs of the simulations are represented by the main dynamic system parameters (velocities, forces, power), which may be used to compare different configurations during the design process.

B. *Simulation based optimization procedure*

A hydrodynamic model has been set up within an optimization procedure with the aim to determine the optimal shape and inertial characteristic of the system for given wave conditions. An optimal configuration is searched by the variation of the following features:

- the shape of the floating body cross-section;
- the mass of the floating body;
- the PTO damping constant.

A starting guess on the position of the centre of gravity and on the principal moment of inertia is assumed.

The goal of the optimization process is the maximization of average power output for the given operating conditions. More details on this part of the work may be found also in [10].

A well-defined shape has been obtained for a regular wave with assigned period and height. The search for an optimized configuration has been more difficult in the case of irregular sea states, where more irregular shapes were generated with lower power improvement.

Optimization has been performed for a regular wave condition with wave amplitude A_w= 0.24 m and frequency f_w=0.35 Hz. In such condition a section shape has been generated together with a given required mass and force-speed gain value. The prototype buoy shape and dimensions, given the operating conditions, were chosen comparing several solutions, using the developed optimization procedure, which was implemented using the ModeFrontier™ commercial code.

It is possible to note a slight similarity between the resulted geometry of the optimization process and the section shape of the Salter's duck device, [11].

III. LARGE SCALE PROTOTYPE TOWING TANK TESTS

C. *Test model*

Based on the optimization results a large-scale model of the system has been developed, in cooperation with Umbra, within a research program supported by WES organization (Wave Energy Scotland).

A picture of the model installed in the towing tank is reported in Fig. 3.

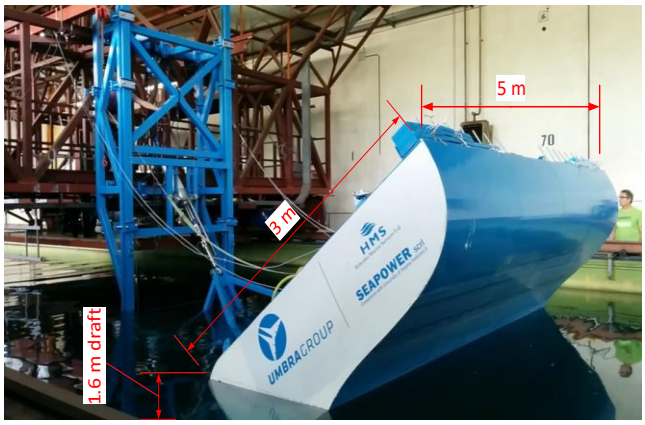

Fig. 3. Large scale test model installed in the towing tank of the University of Naples.

The model, to be tested in controlled environment, was designed in a 1:1 scale with respect to a sea trial demonstrator with a 5 m wide floating body. The total mass of the moving part of the system is about 4760 kg and the immersed volume at rest is equal to 5 m^3. Tests have been performed at the University of Naples, in the towing tank of the Industrial Engineering Department, which is equipped with a wave maker system able to reproduce a large range of wave conditions in regular and irregular sea states. The basin is 130 m long, 9 m wide and has a depth of 4 m. The wave maker of the naval tank is composed by a series of 8 paddles separately actuated and controllable and is able to generate regular and irregular waves, with maximum amplitudes depending on frequency.

The test model is mounted, through a fixed support structure, on the towing cart of the tank, which during these tests was held fixed approximately at the centre of the basin, exposed to the action of the generated wave field.

Some modifications to the configuration obtained from the optimization phase have been implemented in order to improve the integration with the final PTO design. In particular, a connection structure has been interposed between the arms and the PTO lower end in order to reduce the length of the piston.

To implement the PTO control strategy, a simple electrical resistance load is connected at the generator output. A suitable resistor bench has been used in order to adjust the electrical load at the desired level and to test the effect of load variation. It has to be noted that bench tests on the PTO using the resistive load, performed by the constructor, have shown a dependence of the effective force-speed gain on the oscillation velocity. As a consequence, the force-speed gain is not constant during the oscillation; thus, the control law does not exactly comply with the specification in eq. (2) and some discrepancies with the numerical model may be expected.

D. *Test parameters*

The main electrical and mechanical parameters have been collected by the acquisition system during the test execution and visually displayed to control system behaviour and prevent eventual excessive response.

During each test, data were recorded via a LabView™ controlled acquisition system, developed for the towing tank sensor equipment. The system was set up to record data at a sampling frequency of 200 Hz for the following mechanical data:

- wave gauges: a set of 9 wave gauges has been installed along the basin in order to measure the wave field 15 m ahead of the buoy;
- load cells: a load cell has been used to measure the force on the PTO piston (moreover a set of tri-axial load cells has been mounted between the buoy and the supporting arms);
- buoy displacement: in order to determine the elongation of the piston, an LVDT (Linear Variable Displacement Transducer) sensor has been mounted between the piston and the part of the PTO linked to the fixed structure.

The acquisition frequency was increased to 2 KHz for the electrical data from the resistor bench:

- phase currents
- phase voltage

The electrical parameters have been measured by means of current and voltage transducers. From the measured voltages and currents, the instantaneous electric power output can be estimated.

Data were then transferred from the DAQ workstation for further post-processing.

Tests have been performed both in regular and irregular waves.

The test basin was characterized by a preliminary calibration campaign. In particular, using a set of several capacitive wave gages, the reflection coefficient was estimated as the ratio of reflected to incident wave amplitude, for the range of frequency of interest. For regular waves, at the lowest frequencies, around 0.25 Hz, the reflection coefficient was about 0.15. A reduction of the reflection effect with increasing wave frequency was observed up to about 0.6 Hz, where the reflection coefficient reached a value of about 0.02. A further increase was observed for larger frequencies, outside of the tested range. For irregular sea states a larger value of the reflection coefficient was observed, with values ranging from 0.79 to 0.38 in the peak period range between 1.25 s and 4 s.

E. *Regular wave tests*

A matrix of the tested conditions is reported in Table I, which indicates the tested wave amplitude for each frequency and for the considered electrical loads. In table header an approximate correspondence between the electrical load and the PTO force-speed gain (see par. D) is also indicated. It has to be noted that, for the lowest force speed gain, the higher wave amplitude cannot be tested, due to the large oscillations observed, exceeding the PTO stroke limits.

TABLE I
TESTED REGULAR WAVE CONDITIONS

Electrical load	R=1.5 Ω (K≅170 kNs/m)	R=2.5 Ω (K≅110 kNs/m)	R=3.5 Ω (K≅90 kNs/m)	R=4.5 Ω (K≅75kN s/m)	R=5.5 Ω (K≅70 kNs/m)
Wave frequency (Hz)	Tested wave amplitude (m)				
0.3	0.1-0.15	0.1-0.12	0.1-0.15	0.1-0.15	0.1-0.15
0.33	0.1-0.15-0.2	0.1-0.15-0.2	0.1-0.15-0.2	0.1-0.15-0.2	0.1-0.15
0.35	0.1-0.15-0.2	0.1-0.15-0.2	0.1-0.15-0.2	0.1-0.15	0.1-0.15
0.4	0.1-0.15-0.2	0.1-0.15-0.2	0.1-0.15-0.2	0.1-0.15-0.2	0.1-0.15
0.45	0.1-0.15-0.2	0.1-0.15-0.2	0.1-0.15-0.2	0.1-0.15	0.1-0.15
0.50	0.1-0.15-0.2	0.1-0.15-0.2	0.1-0.15-0.2	0.1-0.15	0.1-0.15
0.55	0.1-0.15-0.2	0.1-0.15-0.2	0.1-0.15-0.2	0.1-0.15	0.1-0.15

Buoy performance is represented by the average mechanical power (P_{mech}), obtained at the generator input shaft and here calculated as the product of piston force (measured by the piston load cell) and shaft oscillation velocity (the oscillation velocity was evaluated as the derivative of piston displacement measured by the LVDT mounted on the PTO piston).

A typical time history of the generated power is reported in Fig. 4, which shows both the electrical and

mechanical power outputs for the highest tested wave amplitude (A_w = 0.24 m, with frequency f_w = 0.35 Hz).

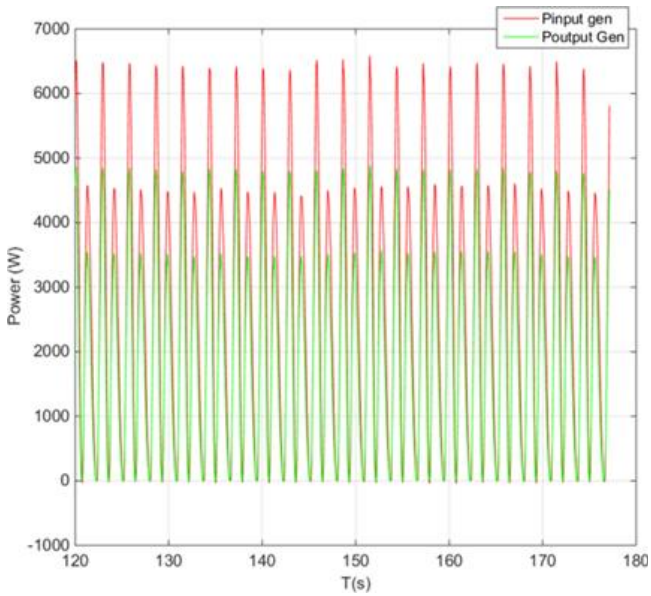

Fig. 4. Typical time histories of measured power at the generator input shaft (red) and at the electrical output (green). Wave amplitude 0.24 m, frequency 035 Hz, electrical load 3.5 Ohm (K=90 kNs/m).

A peak mechanical power output of about 6.5 kW has been observed, while the measured peak electrical power was equal to 4.9 kW. Average and peak power differ by a factor greater than 2. The observed average mechanical power in the same test is, indeed, equal to about 2.6 kW.

It has to be noted that a significant dependence on wave frequency has been observed, as expected for a resonating behaviour. The power production rapidly decreases away from the power production peak frequency (about 0.35 Hz, but variable with the PTO damping). In fact, a major effect of the electrical load (related to the PTO damping) on power performances has also been observed, with significant variations both of the maximum output power and of the optimal frequency. To introduce a global indicator of the conversion efficiency, the wave-to-wire efficiency, η_{tot}, is defined as the ratio of electrical power, P_{elec}, to wave input power, P_{wave_ref}:

$$\eta_{tot} = P_{elec}/P_{wave\,ref} \tag{5}$$

which collectively accounts for the efficiencies along the whole energy conversion chain (wave-to-mechanical power conversion and mechanical-to-electrical power conversion). The reference wave power is calculated as the wave power per unit crest width, P_{wave}, times the width of the floating body, B = 5 m, according to the following relation [11], for regular waves:

$$P_{wave\,ref} = P_{wave}B = \rho_w g H_w^2 c_g/8 \tag{6}$$

where c_g is the group velocity for the given frequency and water depth, and $H_w = 2A_w$ is the wave height.

In Fig. 5, Fig. 6 and Fig. 7 the experimental global efficiency has been reported as a function of frequency for the different tested values of the electrical load, R_{phase} , approximately corresponding to a given force-speed gain, K. It may be noticed that, at least in the interval of the tested resistive loads, the maximum efficiency is reached for higher loads and lower force-speed gains. Continuing in the reduction of the gain, below the minimum testable value, a maximum value is expectable. Moreover, by increasing the gain, the point of maximum efficiency moves towards higher frequencies. For example, at K = 70 kNs/m, the maximum efficiency is obtained at about 0.35 Hz, whereas at K = 170 kNs/m the optimal frequency shifts to about 0.5 Hz.

In the range of tested loads and frequencies, a smaller effect of amplitude on conversion efficiency may be observed. It has to be noted, however, that, for larger oscillations, non-linearity effects may be expected, due to kinematic and hydrodynamic effects, potentially reducing actual efficiencies.

A maximum efficiency of about 0.61 has been observed for K=70 kNs/m at the tested amplitude A_w=0.1 m and a maximum value of about 0.64 has been observed at 0.15 m amplitude with K= 70 kNs/m.

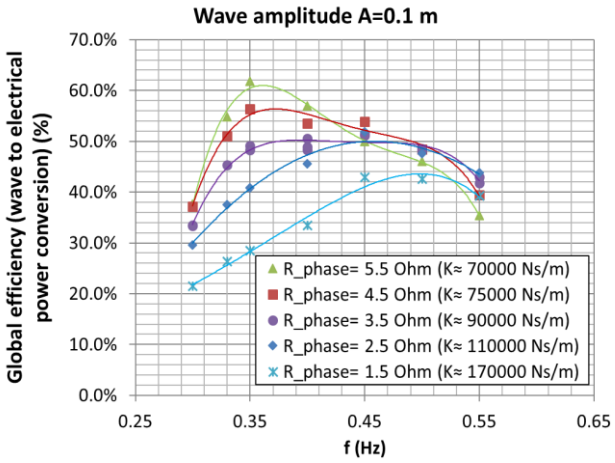

Fig. 5. Wave-to-wire efficiency, in regular wave for wave amplitude A_w = 0.1 m, variable frequency and PTO damping.

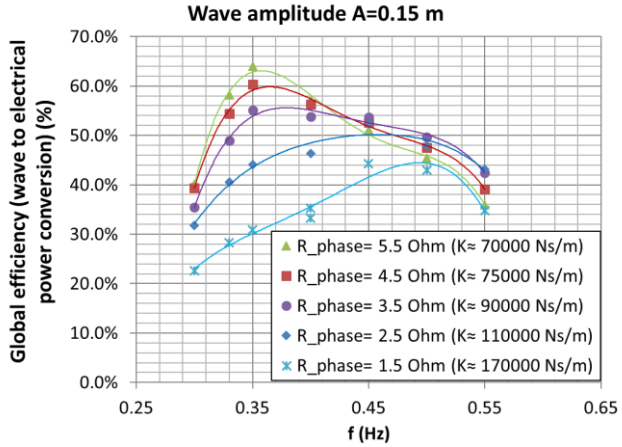

Fig. 6. Wave-to-wire efficiency, in regular wave for wave amplitude A_w = 0.15 m, variable frequency and PTO damping.

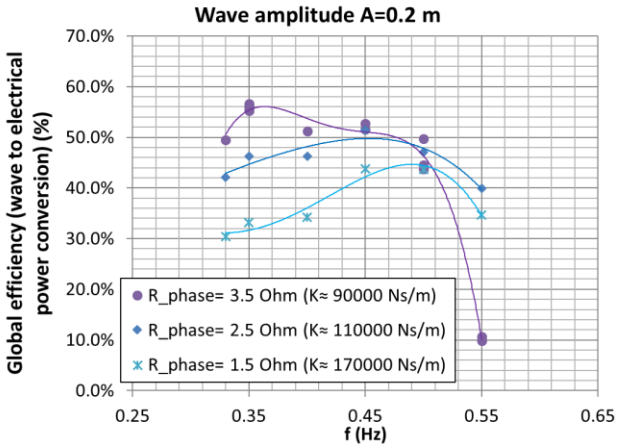

Fig. 7. Wave-to-wire efficiency, in regular wave for wave amplitude A_w = 0.2 m, variable frequency and PTO damping.

For the case K =70 kNs/m (R_{phase} =5.5 Ohm), with amplitude A_w=0.15 m, Table II reports the maximum and average power and the total conversion efficiency, η_{tot}, together with the two separate contributions to the overall conversion chain efficiency:

- buoy-to-mechanical energy conversion efficiency ($\eta_{mech} = P_{mech}/P_{wave\,ref}$)
- mechanical-to-electrical energy conversion efficiency ($\eta_{PTO} = P_{elec}/P_{mech}$)

TABLE II
POWER OUTPUT DATA FOR TESTS WITH WAVE AMPLITUDE A_W=0.15 m AND FOR AN ELECTRICAL LOAD R_{phase}=5.5 Ohm (K=70 KNs/m)

f (Hz)	P_{wave} (kW)	P_{mech} Max. (kW)	P_{mech} Avg. (kW)	P_{elec} Max (kW)	P_{elec} Avg. (kW)	η_{mech}	η_{PTO}	η_{tot}
0.300	1.67	2.63	0.89	1.63	0.67	0.532	0.753	0.401
0.330	1.47	2.90	1.11	2.13	0.86	0.756	0.770	0.582
0.350	1.35	2.94	1.13	2.20	0.87	0.831	0.770	0.640
0.400	1.13	2.09	0.84	1.55	0.64	0.747	0.763	0.570
0.450	0.97	1.45	0.66	1.13	0.50	0.675	0.757	0.511
0.500	0.87	1.18	0.52	0.86	0.39	0.605	0.750	0.454

A very large estimated buoy efficiency (about 83%) may be observed. It has to be noted, however, that such values may be affected by the interaction with the wall of the test basin. The ratio, r_B, of the floating body width (B=5 m) and the tank width (B_{basin}=9 m) is equal to r_B=0.56. Moreover, the values of the efficiency are strongly dependent on the electrical load (or the force-speed gain).

Also, the PTO efficiency is significantly affected by the electrical load, whereas the dependence on frequency is less evident, with a typical value in the above reported cases of about 75%.

F. *Irregular wave tests*

A second phase of the test campaign has been dedicated to the tests in irregular sea states. With the same test arrangement used for the regular wave tests, a set of wave spectra has been considered.

The main difference between regular and irregular tests is related to the length of the test runs. For regular waves, tests were about 4 minutes long and 20 wave cycles were considered to assess the buoy and PTO performance, after a settling time of about 60 seconds. For irregular sea states, 10 minutes' runs are considered and calculations start after a settling time of 60 seconds after the first wave passed the buoy.

To model the spectral energy distribution, the JONSWAP and Pierson-Moskowitz analytical spectra have been used [12], [13]. The Pierson-Moskowitz spectral model used during the tests may be expressed using the following relation:

$$S_{PM}(\omega) = \alpha H_s^2 \omega_p^4 \omega^{-5} \exp\left(-\frac{5}{4}\left(\frac{\omega}{\omega_p}\right)^{-4}\right) \quad (7)$$

The JONSWAP spectrum has the following expression:

$$S_J(\omega) = A_\gamma S_{PM}(\omega) \gamma^{exp\left(-0.5\left(\frac{\omega-\omega_p}{\sigma\omega_p}\right)^2\right)} \quad (8)$$

and it reduces to the Pierson-Moskowitz spectrum when the constant γ, a non-dimensional peak shape parameter also indicated as "peakedness factor", is equal to 1. Typical values for the constants present in the JONSWAP experimental data are γ = 3.3 (variable in the range from 1.0 to 7.0 approximately), σ= 0.07 for $\omega \leq \omega_p$, σ= 0.09 for $\omega > \omega_p$ (where ω_p is the peak spectral circular frequency). Larger values of γ correspond to a narrower spectrum. A_γ is a normalization constant equal to $A_\gamma = 1 - 0.287\ ln(\gamma)$.

Several sea states and loading conditions have been tested throughout the campaign, exploring the effects of different parameter variations. During the tests the spectral parameters have been changed allowing to study the effects of different sea states. Two parameters are used to characterize the spectra:

- the significant wave height, defined as
$$H_s = 4\sqrt{m_0}$$
where m_0 is the variance of the sea surface elevation;
- the peak period of the spectrum, T_p, or its related angular frequency, ω_p, and frequency, f_p.

Also, in irregular waves a measure of the conversion efficiency is estimated as the ratio of average output power to the wave reference spectral power content. An estimation of average wave power per unit width for irregular waves may be obtained using the following relation [1]:

$$P_{wave\ spectrum} = \frac{\rho g^2}{64\pi} H_s^2 T_e \quad (9)$$

where T_e is the energy period, which may be defined in terms of spectral moments and may be related to the peak period for a given spectrum shape (for indications about

spectra related definitions, see for example [13], [12]). The measured peak frequency and significant height have been used to evaluate the wave transported power.

1) Effect of PTO damping (electrical load)

The effect of load resistance variation has been tested for two sea states, with significant energy content and complying with the operational limits of the test system. The two tested Pierson-Moskowitz spectra have the following spectral characteristics:

- H_s=0.2 m, T_p=2.5 s (f_p=0.4 Hz)
- H_s=0.3 m, T_p=2.857 s (f_p=0.35 Hz)

Fig. 8 reports the trend of the average mechanical power for the two tested spectra at variable electrical loads.

It has to be noted that lower average power values are observed, in comparison with regular wave test results, as expected due to the irregular nature of the sea state. Instantaneous peak power reaches larger value, comparable with the peak value observed in the regular wave tests.

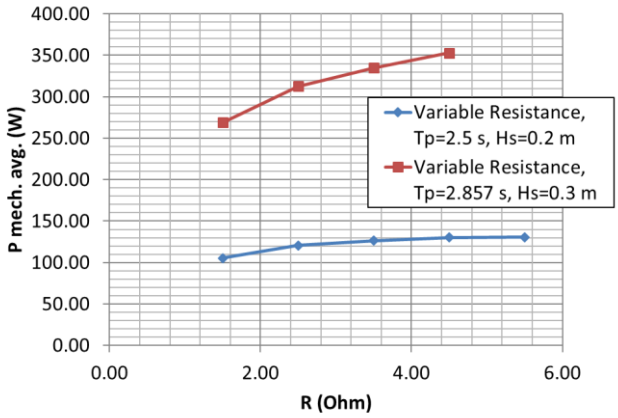

Fig. 8. Mechanical avg. power as a function of electrical load for two different Pierson-Moskowitz spectra: H_s=0.2 m, T_p=2.5 s (blue); H_s=0.3 m, T_p=2.857 s (red).

The global efficiency is reported in Fig. 9 for the considered spectra and electrical load range (PTO damping).

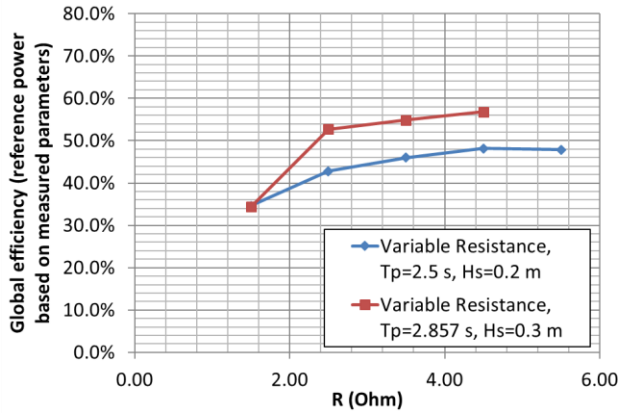

Fig. 9. Global efficiency as a function of electrical load for two different Pierson-Moskowitz spectra: H_s =0.2 m, T_p =2.5 s (blue); H_s=0.3 m, T_p=2.857 s (red).

Lower values of the overall conversion efficiency, in comparison with regular waves, may be observed in the case of irregular sea states, with maximum values ranging in the interval 48% ÷ 56%.

2) Effect of spectral peak frequency

To explore the effect of the spectrum peak period, a set of tests has been performed with two types of spectra: P-M and JONSWAP (with the default value of γ=3.3). The electrical load is fixed to a value of R_{phase} =3.5 Ohm (approximately corresponding to a PTO damping value equal to K=90 kNs/m).

As in regular wave tests, also in this case it is possible to note a large difference between the average and peak values of power output, as shown in Fig. 10. In this case, the peak-to-average power ratio is even higher, with peak power up to about 20 times larger than the average.

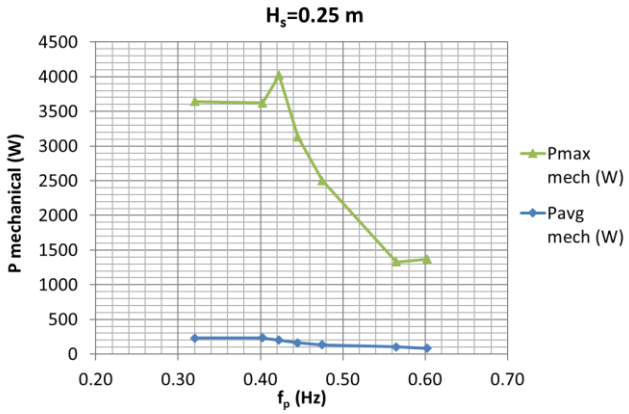

Fig. 10. Average and peak mechanical power for Pierson-Moskowitz spectrum, with H_s=0.25 m for different peak frequency.

The estimated conversion efficiency is reported in Fig. 11. The maximum conversion efficiency in these tests reached a value of about 54%. A decreasing trend with peak frequency may be observed in the tested frequency range, starting from a value of about 0.35 – 0.4 Hz.

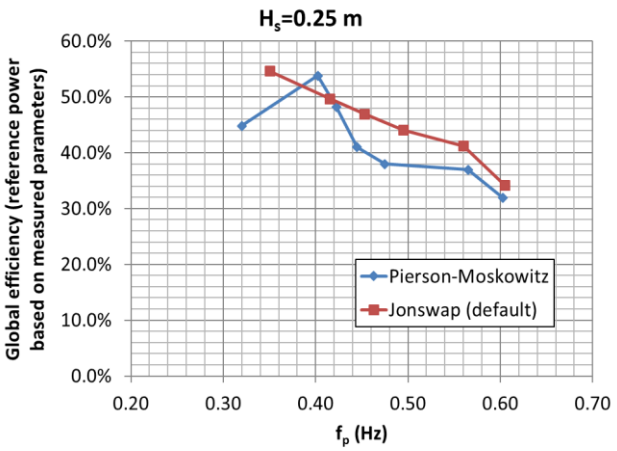

Fig. 11. Global efficiency as a function of spectrum peak frequency for JONSWAP and Pierson-Moskowitz spectra for H_s=0.25 m, with R_{phase}=3.5 Ohm (K=90 kNs/m).

3) Effect of spectrum shape

Finally, changing the value of the peak enhancement factor, γ, for a JONSWAP spectrum, the effect of spectrum shape may be investigated, in particular with respect to the effect of spectral width.

As can be observed from Fig. 12, increasing γ yields a slight increase in global conversion efficiency. For narrower spectra (larger γ), the efficiency approaches values closer to the ones obtained for regular waves.

G. Observations on power production tests

The performed tests have mainly highlighted a potential overall conversion efficiency of about 55% in irregular sea states, with a significant reduction in comparison to regular wave tests. Moreover, the large differences between peak and average power output may introduce severe limitations to the operation of the system.

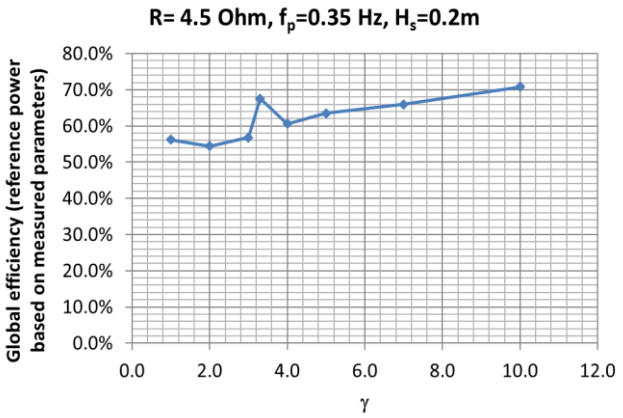

Fig. 12. Global efficiency as a function of spectrum peak enhancement factor, γ, for JONSWAP spectrum with H_s=0.2 m, for R_{phase}=3.5 Ohm (K=90 kNs/m).

The agreement of experimental results with numerical prediction (potential theory model) is reasonably good, as can be seen from Fig. 13 and Fig. 14 for regular and irregular waves respectively.

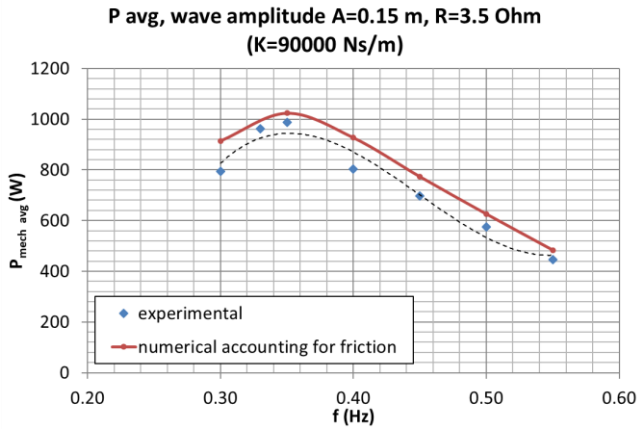

Fig. 13. Numerical-experimental comparison. Regular wave, A=0.15 m, K=90 kNs/m

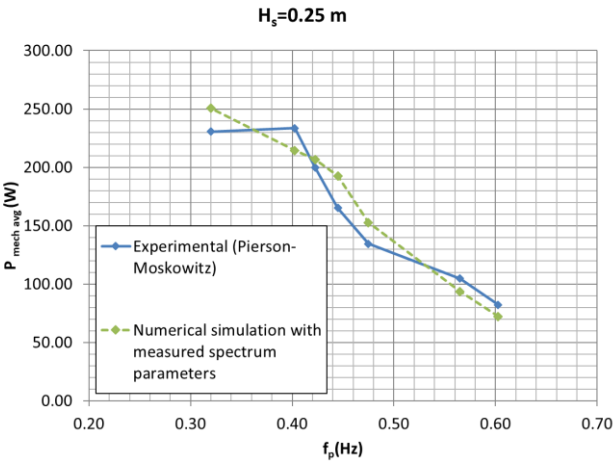

Fig. 14. Numerical-experimental comparison. Irregular waves, H_s=0.25 m, K=90 kNs/m. Pierson-Moskowitz spectrum.

It has to be noted, however, a certain discrepancy between predictions and measures, which may also increase in other conditions. Such differences may be explained in part with the effect of viscosity (neglected in the model) and in part with the approximation in realizing the linear control law by means of the resistive electrical load.

IV. Preliminary Studies for a Sea Trial Prototype

The project was expected to proceed in few months from the date of writing with the installation of a large-scale prototype to be deployed on a coastal structure in the Civitavecchia harbour, to undertake a brief preliminary series of sea trials.

A structure has been designed based on the load predictions from the developed and tested simulation model.

One of the objectives of the designed support structure is to ensure the survivability under extreme wave loading. In such conditions, the system has to be placed in a non-operating protection state. After considering several possible solutions, a lifting device based on an articulated quadrangle mechanism has been designed, as described in Fig. 15.

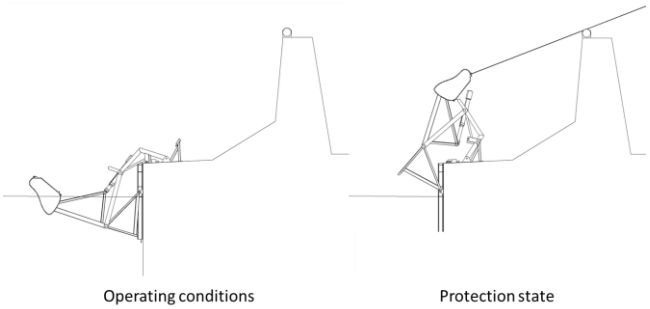

Fig. 15. Onshore WEC system mounted on a breakwater structure. During operations (left). In protection state for extreme waves (right).

The lifting system is connected to an existing fixed harbour structure, such as a breakwater with a given wall section shape.

H. Tests on breakwater mounted structure

In order to study the effective loading conditions, a set of experimental tests have been performed, in the towing/wave tank of the University of Naples, on a small model of a structure mounted on a breakwater in the protection position (as shown in Fig. 15(right)). Due to a reduced amount of literature data about the estimation of the actions on a wall mounted structure, a preliminary experimental campaign was set-up. A 1:44 wooden model of the breakwater section present at the installation site has been built. On the wall model, a small structure in the same scale was mounted and equipped with a load cell in order to measure the forces due to the wave action, also accounting for the interaction with surrounding breakwater. Capacitive wave gages were used to measure the height of the incoming wave and the local elevation of water surface near the wall.

Fig. 16 illustrates the installation of the test model in the wave tank. A rectangular beam, with dimensions 5×28×270 mm, mounted on a load cell, was used in a first set of tests to obtain a measure of wave forces. The vertical wall has a width of 2 m and a depth of 1.4 m.

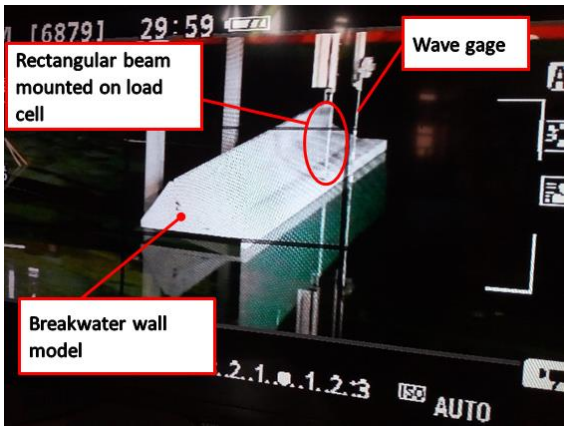

Fig. 16. Test model of the breakwater mounted structure, installed in wave tank.

TESTS ON A BAR MOUNTED ON A LOAD CELL

The tests were carried out, for the largest part, under regular wave conditions. In most of the tests, a bar was used as a simplified representation of a body subject to wave action in presence of a vertical wall. Some tests have also been performed on a small scale (1:44) model of the WEC system in the protection position.

For the tests on the load-cell mounted bar, the conditions indicated in Table III have been investigated.

The maximum wave height corresponds in scale to a real height of about 8.8 m (indication on scaling may be found in [14]), which, from previous wave climate studies, is expected as the most probable maximum height for a sea state with a 5 year return period, associated to a wave period of approximately 9.5 s.

TABLE III
TESTED WAVE CONDITIONS

Wave height		Frequency	
Model (mm)	Real scale (m)	Model (Hz)	Real scale (Hz)
40	1.76	0.3 – 1.2	0.0452 – 0.1809
60	2.64	0.3 – 1.0	0.0452 – 0.1508
80	3.52	0.3 – 1.1	0.0452 – 0.1658
100	4.40	0.3 – 1.1	0.0452 – 0.1658

A significant increase in surface elevation has been observed near the wall, as an expected consequence of wall reflection. The following Fig. 17 shows a summary of the measured maximum surface elevation at the wall for three frequencies and for the tested incoming wave amplitudes.

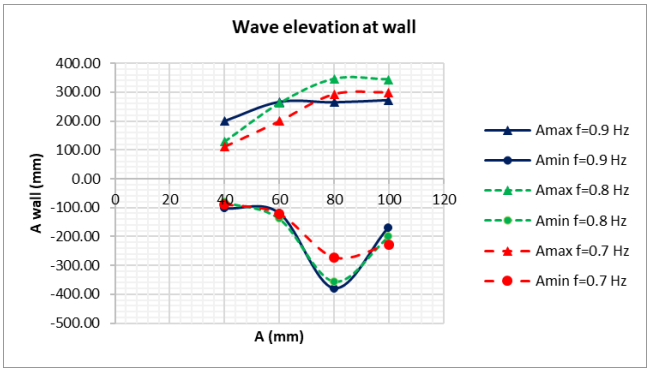

Fig. 17. Measured surface elevation (maximum and minimum) at wall for 0.7, 0.8 and 0.9 Hz and different amplitude. Rectangular bar model.

As can be seen form Fig. 17, an asymmetric behaviour between crest and valleys has been observed with generally deeper troughs near the wall. Also, some irregularity in the trend may be observed, with a larger trough for 80 mm amplitude than for 100mm.

Moreover, probably due to the finite width of the wall, the surface height, as well as the measured forces, show a peak at a single frequency, between 0.7 and 0.9 Hz, as shown for the case of 100 mm amplitude in Fig. 18.

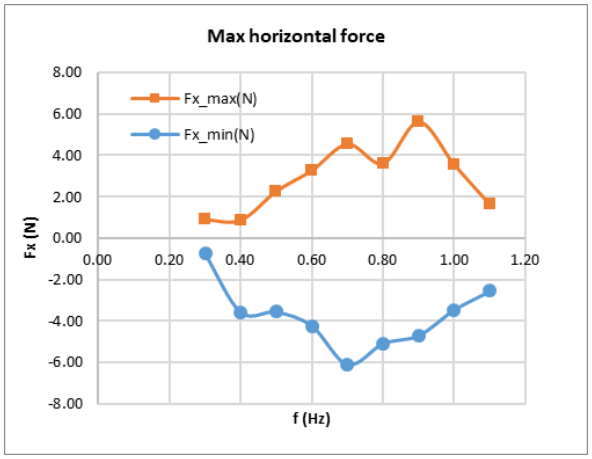

Fig. 18. Measured max horizontal force (maximum and minimum) as a function of frequency, for 100 mm amplitude (corresponding to 4.4 m amplitude in real scale). (Negative sign for backward acting forces). Rectangular bar model.

An irregular behavior may be observed in the data trend as a function of frequency, probably due in part to vibrations of the supporting structure and in part to the very irregular wave field observed in the vicinity of the reflecting wall. Moreover, the presence of a peak frequency may be noted, which may be influenced by the finite transverse extension of the vertical wall used in the experimental set-up. Further investigations are needed.

TEST ON 1:44 WEC MODEL

Tests on the 1:44 WEC scaled model in protection state have been performed around the 0.7 Hz frequency, corresponding to a real scale wave period of about 9.5 s. Results are reported in Table IV, in terms of wave elevation at the wall and horizontal force on the model. Forces are measured with a load cell, on which the WEC model is mounted. Care has been taken to place the model as close as possible to the wall, but preventing possible contacts.

TABLE IV
MEASURED SURFACE ELEVATION AT WALL AND HORIZONTAL FORCES ON THE 1:44 SCALED WEC MODEL

Wave amp. A (mm)	*Wave period* T (s)	*Max surface elevation at wall* (mm)	*Min surface elevation at wall* (mm)	*Max Hor. force* (N)	*Min Hor. forcer* (N)
60	1.429	197.02	-122.74	1.63	-1.42
80	1.429	290.03	-310.64	4.67	-1.68
100	1.429	345.09	-344.06	4.85	-2.44
100	1.250	343.98	-377.95	5.62	-4.70

An estimation of the loads on the real scale structure may be obtained by using Froude scaling laws [14] according to the following relation:

$$F_{real\,scale} = s^3 F_{model} \tag{10}$$

where s is the geometric scale (1:44 in the present case).

TABLE V
HORIZONTAL FORCES ON REAL SCALE WEC (SCALED BY FROUDE LAW)

Wave amp. A (m)	*Wave period* T (s)	*Max Hor. force* (kN)	*Min Hor. forcer* (kN)
2.64	9.48	139.1	-120.8
3.52	9.48	397.8	-143.1
4.4	9.48	413.3	-208.0
4.4	8.29	478.8	-400.0

In the preceding table wave amplitudes and periods have also been estimated by using Froude scaling laws, according to the following relationships:

$$T_{real} = s^{1/2}\, T_{model} \tag{11}$$

$$A_{real\,scale} = s\, A_{model} \tag{12}$$

The scaled estimations reported before are referred to a buoy with a width of $B_{real\,scale} = sB_{model} = 5$ m.

As can be seen, a very large horizontal force is expected on the real structure in extreme wave conditions. Even for a limited return period (5 years), the expected force is approximately equal to 480 kN, thus requiring a very robust and expensive structure. This condition appears to be one of the most demanding problems for the development of the project.

V. CONCLUSIONS

The main results of the research activities for the development of a WEC device have been presented in the present paper. Experimental tests on a large-scale model (with a 5 m wide floating body) in controlled environment have shown a promising overall efficiency. In view of the deployment of a prototype in real sea environment on a harbour structure, a protection system for extreme wave conditions has been studied. Some experimental tests on a small-scale model (1:44) of the system installed on a vertical wall structure were performed, highlighting the severe loads expected under extreme waves.

REFERENCES

[1] J. Falnes, Ocean Waves and Oscillating Systems, Cambridge Univesity Press, 2002.
[2] R. Hager, N. Fernandez and M. H. & Teng, "Experimental Study Seeking Optimal Geometry of a Heaving Body For Improved Power Absorption Efficiency," in *Proceedings of the 22nd International Offshore and Polar Engineering Conference (ISOPE 2012)*, Rhodes, Greece, 2012.
[3] M. Vantorre, R. Banasiak and R. Verhoeven, "Modelling of hydraulic performance and wave energy extraction by a point absorber in heave," *Applied Ocean Research,* pp. 61-72, February 2004.
[4] L. Marquis, M. Kramer and P. Frigaard, "First Power Production figures from the Wave Star Roshage Wave Energy Converter," in *ICOE, 3rd International Conference on Ocean Energy*, Bilbao, 2010.
[5] J. Hardisty, "Experiments with point absorbers for wave energy conversion," *Journal of Marine Engineering & Technology,* pp. 51-62, 2012.
[6] D. Ionescu and B. Ngwenya, "Innovative Design of a Sea Wave Energy Harnesser," in *International Conference on Renewable Energies and Power Quality (ICREPQ'14)*, Cordoba (Spain), 2014.
[7] O. M. Faltinsen, Sea Loads on ships and offshore structures, Cambridge University Press, 1990.
[8] H. O. Berteaux, Engineering, Buoy, Wiley-Interscience, 1976.
[9] D. P. Coiro, G. Troise, G. Calise e N. Bizzarrini, «Wave energy conversion through a point pivoted absorber: Numerical and experimental tests on a scaled model,» *Renewable Energy,* 2015.
[10] D. P. Coiro, G. Troise, G. Calise e N. Bizzarrini, «Experimental test and numerical shape optimization of a point pivoted absorber for wave energy,» in *VI International Conference on Computational Methods in Marine Engineering, Marine 2015*, Rome, Italy, 2015.
[11] S. Salter, «Wave power,» *Nature,* vol. 249, pp. 720-724, 1974.
[12] M. McCormick, Ocean Wave Energy Conversion, Annapolis, USA: Dover, 2007.
[13] DNV, «Environmental Conditions and Environmental Loads,» 2014.
[14] ITTC Specialist Committee on Waves, «Final Report and Recommendations to the 23rd ITTC,» in *Proceedings of the 23rd ITTC – Volume II*, Venice, Italy , 2002.
[15] G. Payne, «Guidance for the experimental tank testing of wave energy converters,» SuperGen Marine, Edinburgh, 2008.